JGR Oceans

RESEARCH ARTICLE

10.1029/2025JC023742

Thermal vs. Haline Drivers of Restratification in the Labrador Sea

H. Jaques[1,2], L. Clément[1], E. Frajka-Williams[3], A. C. Naveira Garabato[2], and M. Oltmanns[1,4,5]

[1]National Oceanography Centre, Southampton, UK, [2]University of Southampton, Southampton, UK, [3]University of Hamburg, Hamburg, Germany, [4]Alfred Wegener Institute - Helmholtz Centre for Polar and Marine Research, Bremerhaven, Germany, [5]University of Bremen, Bremen, Germany

Key Points:

- Salinity dominates early winter stratification in December, while temperature has a destabilizing influence from January onwards
- Restratification from mid-March coincides with a transition back toward salinity-determined stratification
- Submesoscale freshwater fronts are predominant during restratification, rather than warm fronts

Correspondence to:

H. Jaques,
hlj1n22@soton.ac.uk

Citation:

Jaques, H., Clément, L., Frajka-Williams, E., Garabato, A. C. N., & Oltmanns, M. (2026). Thermal vs. haline drivers of restratification in the Labrador Sea. *Journal of Geophysical Research: Oceans*, *131*, e2025JC023742. https://doi.org/10.1029/2025JC023742

Received 14 NOV 2025
Accepted 7 MAY 2026

Author Contributions:

Conceptualization: H. Jaques, L. Clément
Data curation: H. Jaques, L. Clément, E. Frajka-Williams
Formal analysis: H. Jaques
Funding acquisition: E. Frajka-Williams
Investigation: H. Jaques, L. Clément, E. Frajka-Williams
Methodology: H. Jaques, L. Clément
Resources: L. Clément, E. Frajka-Williams
Supervision: L. Clément, E. Frajka-Williams, A. C. Naveira Garabato, M. Oltmanns
Visualization: H. Jaques
Writing – original draft: H. Jaques
Writing – review & editing: H. Jaques, L. Clément, E. Frajka-Williams, A. C. Naveira Garabato, M. Oltmanns

Abstract The Labrador Sea is a vital component of global ocean circulation, hosting vigorous deep convection that can mix to deeper than 2,000 m. Features that drive convection are widely studied, but a lack of high-resolution, in situ observations hinder our understanding of how finescale dynamics influence the convective process and trigger restratification in spring, particularly at the submesoscales (<∼ 10 km). This study assesses contributions of temperature and salinity to both vertical and horizontal stratifications during early winter, convection, and spring restratification, using data collected by five underwater gliders deployed in the winters of 2019/20 and 2021/22. Using the Turner angle, we show that vertical stratification in the Labrador Sea shifts from salinity-stratified in early winter to temperature-unstable during convection, and back to salinity-stratified in the early restratification period. Horizontally, both warm and fresh intrusions drive lateral density anomalies during restratification, with the haline influence dominating. Wavelet analysis of these anomalies illustrates increased submesoscale activity during restratification, and comparisons of thermohaline contributions show the predominance of salinity-driven submesoscale fronts. These fronts have the potential to rapidly stratify the water column, and evidence the importance of freshwater intrusions at submesoscales in halting convection.

Plain Language Summary The Labrador Sea is an important site of deep ocean mixing that plays a major role in the storage of atmospheric carbon and redistribution of heat and oxygen through the ocean. Each winter, strong winds and cold air cool the ocean surface and cause the water column to mix to depths of over 2,000 m. At the end of winter, this mixing stops and the water column stabilizes in a process known as restratification. Little is known about how this restratification occurs, and it is unclear whether inputs of warm vs. fresh waters are more important. To investigate this, five underwater robots collected data across two winters (2019/20 and 2021/22). We found that the saltiness (salinity) of water is the main factor controlling ocean stability during early winter. Later in winter, when strong winds cool the ocean surface, temperature instead becomes more important and helps to drive mixing. However, in springtime, even though cold atmospheric conditions persist, flows of warmer and fresher waters stop this mixing, with the fresher water having a stronger effect. This suggests that, in a warming climate, increased freshwater inputs to the Labrador Sea could have a greater impact on restratification than warming itself.

1. Introduction

Deep ocean convection takes place in limited locations around the world. One of these locations is the Labrador Sea in the subpolar North Atlantic, which experiences convection that can sometimes reach deeper than 2000 m (Marshall et al., 1998). Here, deep convection has an essential role connecting the surface ocean to the interior, ventilating deep waters with oxygen and carbon dioxide, and forming a new water mass named Labrador Sea Water (LSW) (Lazier et al., 2002; Rhein et al., 2017; Sabine et al., 2004). This water mass is transported southwards within the Deep Western Boundary Current and joins the lower limb of the Atlantic meridional overturning circulation (AMOC), making Labrador Sea deep convection a vital influence on AMOC variability, global ocean circulation, and heat transport (Böning et al., 2006; Talley, 2003; Yashayaev et al., 2007; Yeager et al., 2021). Therefore, understanding the processes involved in the deep convection lifecycle is important for our knowledge of the wider North Atlantic circulation and climate.

Open-ocean deep convection in the Labrador Sea is made possible through the combination of preconditioning of the water column and atmospheric conditions each winter. The cyclonic circulation of the basin weakens the

vertical stratification by doming isopycnals toward the surface. This, alongside weaker stratification from successive years of deep mixing, creates conditions favorable for convection to take place (Clarke & Gascard, 1983; Lavender et al., 2000; Marshall & Schott, 1999; Pickart et al., 2002; Våge et al., 2009). Following this, buoyancy losses at the ocean surface destabilize the water column and enable deep mixing. These buoyancy losses occur over the winter period primarily due to the removal of heat, which is driven by strong winds from North America and Greenland. These winds bring cold and dry air over the surface of the Labrador Sea, producing sensible and latent heat fluxes that sometimes exceed 700 W m^2 (Marshall & Schott, 1999; Schulze et al., 2016). Therefore, years of strong atmospheric forcing or preconditioning tend to occur alongside periods of extensive deep convection, such as during the winters of 1972, 2007/08, and 2015/16 (Uppala et al., 2005; Våge et al., 2009; Yashayaev & Loder, 2016).

While buoyancy losses from surface ocean cooling destabilize the water column, there is a subtle balance between temperature and salinity stratifications that can control the ability for the water column to overturn. A major example of salinity stratification is the Great Salinity Anomaly (GSA) of 1968–1972, and later the lesser GSA between 1980 and 1983, during which freshwater anomalies halted deep convection in the Labrador Sea (Belkin et al., 1998; Curry et al., 1998; Gelderloos et al., 2012). Convection is also limited in the northern and eastern Labrador Sea due to constant replenishment of heat from the boundary currents, and freshwater input from the Greenland and Irminger Seas (Chanut et al., 2008; Clément et al., 2023; Pickart et al., 2002; Schulze et al., 2016). The thermal and haline characteristics of the Labrador Sea therefore have a distinct influence on water column convection and stability. This is also important at the end of winter, where fluxes of heat and freshwater contribute to the restratification of the water column and the overall end of convection (Lazier, 1980; Marshall & Schott, 1999; Straneo, 2006). However, while it is known that transports of fresh and warm waters can end the convective process, there are limited observations of restratification in the Labrador Sea. This is due to the harsh winter conditions, which make gathering in situ observations difficult. As a result, the mechanisms via which restratification happens, and the relative importance of the thermal and haline contributions, remain unclear.

Initial research on Labrador Sea restratification theorised that instabilities around the convective patch transported buoyant (warm and fresh) waters toward the convective region (Clarke & Gascard, 1983; Jones & Marshall, 1997). Since this time, observational (Hátún et al., 2007; Lilly et al., 2003; Prater, 2002) and modeling (Chanut et al., 2008; Eden & Böning, 2002; Katsman et al., 2004; Spall, 2004) studies have identified the transport of buoyant water from the boundary region via mesoscale eddies. These include Irminger Rings, boundary current eddies and convective eddies (Gelderloos et al., 2011; Rieck et al., 2019). While there is a good understanding of how and where these eddies form, disagreements remain on the relative transports of heat and freshwater that they contribute to the convective patch, and how this shapes restratification. Most of these studies focus on lateral eddy heat transport, while freshwater fluxes are largely unaccounted for, often due to the difficulties in analyzing the evaporation - precipitation balance (Straneo, 2006). Hátún et al. (2007) estimated the freshwater transport, suggesting that Irminger Rings are responsible for 50% of the freshwater transported to the surface layers of the central Labrador Sea. However, uncertainties are high and their Seagliders were unable to sample eddies within the convective region, so it is unclear whether this freshwater was involved in the restratification of the water column or was instead mixed away from the convective patch.

Furthermore, it is also argued that mesoscale eddies are not responsible for the immediate restratification observed within the convective region. Instead, it has been shown in a variety of convective settings that smaller-scale (submesoscale) fronts can become baroclinically unstable and restratify the mixed layer over timescales as short as one day (Boccaletti et al., 2007; Frajka-Williams et al., 2014). For example, Thompson et al. (2016), du Plessis et al. (2019), and Giddy et al. (2021) identified an enhanced presence of submesoscale activity at the end of winter that contributes to restratification. More recently, observations from gliders deployed in the Labrador Sea have also revealed that submesoscale intrusions of both fresh and warm waters can develop symmetric instabilities and lead to restratification of the mixed layer (Clément et al., 2023). This highlights how submesoscale fluxes of heat and freshwater have a role in the rapid restratification of the Labrador Sea. However, we do not know whether small-scale warm and fresh intrusions are contributing equally to the stratification, or whether one component is more important.

Considering that freshwater fluxes from the Arctic and the Greenland Ice Sheet may increase in a future warming climate (Böning et al., 2016; Cosmiso, 2006; Hanna et al., 2008), it is vital to understand how thermal and haline fluxes influence convection dynamics. This study aims to establish how vertical and horizontal stratifications

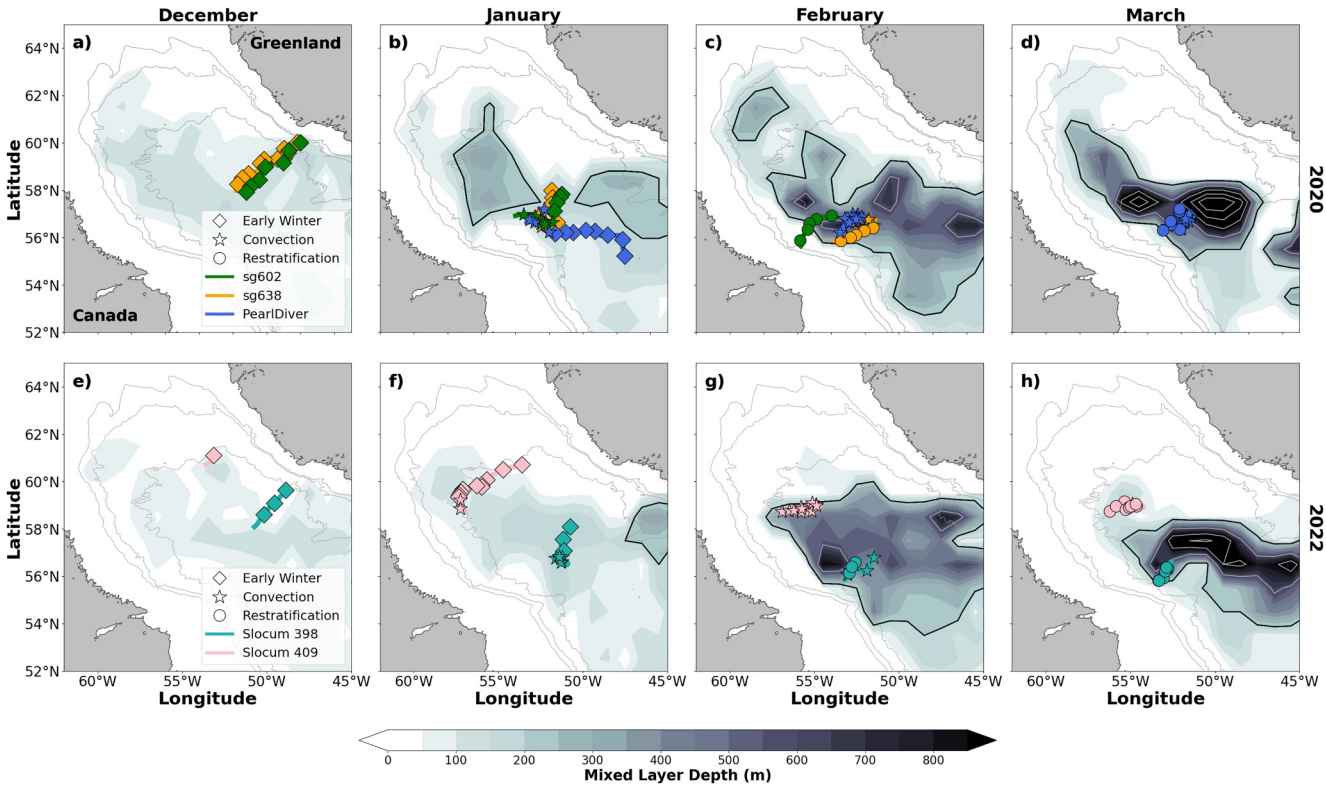

Figure 1. Glider trajectories in the Labrador Sea in winter 2020 (a–d) and 2022 (e–h). The monthly averaged mixed layer depth (MLD) using ARGO climatology (Argo, 2000; Roemmich & Gilson, 2009) is shown in the background. The symbols on the glider tracks represent each winter period; a diamond represents "early winter," a star "convection," and a circle "restratification." Topography data are from the NOAA National Geophysical Data Center (2009). The gray isobaths represent underwater depths of 1,000, 2000, and 3,000 m going from the outside of the basin inwards. The bold black line highlights the 200 m MLD contour.

evolve over the winter season, with a particular focus on the restratification period. Additionally, we wish to investigate the scales of horizontal stratification, and understand whether submesoscale fronts are primarily driven by gradients in temperature or salinity.

2. Methods

2.1. Glider Data

This study investigates how the thermal and haline characteristics of the Labrador Sea influence both vertical and horizontal stratification. To do this, we used data collected by five underwater gliders that sampled the Labrador Sea over two winters (Figure 1). During the first winter of 2019/20 three gliders were deployed, two of which (sg602 and sg638) were Kongsberg Seagliders from the TERIFIC (Targeted Experiment to Reconcile Increased Freshwater with Increased Convection) project. The third glider (Pearldiver) was a Teledyne Slocum glider deployed as part of the HOTSeALS (Heat and Oxygen Transport Sensing Across the Labrador Sea) project. During the second winter of 2021/22 two further gliders were sent out. These were Slocum G2 gliders (398 and 409) also part of the TERIFIC project. For further information on each deployment, see Clément et al. (2023, 2024).

To investigate Labrador Sea dynamics over winter, the glider data were categorized into three sections to enable sub-seasonal comparisons of water column conditions. These periods were "early winter," "convection" and "restratification," and were defined based on the evolution of the mixed layer depth (MLD). The MLD is calculated from a density threshold of 0.01 kg m^{-3} (Piron et al., 2016) relative to a 10 m density value. Early winter begins when the glider enters the Labrador Sea and concludes once the MLD is deeper than 200 m. Convection is defined from this point onwards until the MLD shoals and its daily variability consistently exceeds 80 m (Clément et al., 2023). Restratification then takes place until the MLD remains shallower than 50 m. Each

Table 1
Correlation Between the Temperature and Salinity Contributions to Density for Each Glider and Each Period

	Early winter			Convection			Restratification		
Glider	Dates Start–End	T *r*, slope	S *r*, slope	Dates Start - End	T *r*, slope	S *r*, slope	Dates Start–End	T *r*, slope	S *r*, slope
sg602 2019–20	09 Dec–13 Jan	0.96 1.30	−0.63 −0.31	13 Jan– 01 Feb	0.81 0.82	0.3 0.18	01 Feb–16 Feb	**0.91 1.20**	−0.36 −0.2
sg638 2019–20	09 Dec–14 Jan	0.96 1.43	−0.74 −0.43	14 Jan– 19 Feb	0.77 0.60	0.63 0.40	19 Feb–01 Mar	0.36 0.11	**0.95 0.89**
Pearl 2019–20	05 Jan– 21 Jan	**0.86 0.46**	**0.89 0.54**	21 Jan– 16 Mar	0.37 0.13	0.94 0.87	16 Mar–31 Mar	0.37 0.18	**0.88 0.82**
398 2021–22	19 Dec–09 Jan	0.28 0.20	0.77 0.80	09 Jan– 19 Feb	0.81 1.22	−0.24 −0.22	19 Feb– 01 Apr	0.20 0.11	**0.86 0.89**
409 2021–22	28 Dec–27 Jan	**−0.81–0.18**	**0.99 1.18**	27 Jan– 02 Mar	**0.75 0.33**	**0.92 0.67**	02 Mar–04 Apr	0.16 0.07	**0.90 0.93**

Note. Significant correlations (for $p < 0.05$) are shown in bolded red.

glider traveled through the Labrador Sea with varying trajectories (Figure 1), and consequently collected data for each of these winter periods at various times and locations. As such, the 'restratification' period can represent a local change in MLD sampled by a glider (e.g. Pearldiver, Figure 1d) or the glider can sample a varying MLD when escaping the convective patch (e.g. sg602 and sg638, Figure 1c).

Early winter began during December for all gliders except Pearldiver, where this period started on 5 January 2020. During early winter, glider 409 traveled southwestward at the northern edge of the convective patch (Figure 1f), whereas all other gliders were positioned more centrally in the Labrador Sea between 56°N and 58°N (Figures 1b and 1f). All gliders began to measure convection during January and continued to do so for the remainder of the month (see Table 1 for exact dates of each winter period). Gliders sg602 and sg638 began to measure restratification as they traveled westward toward the Labrador Shelf, meaning that the restratification they observed is spatial as the gliders approached the edge of the convective patch. In contrast, Pearldiver and gliders 398 and 409 remained within known convective areas during their restratification periods, and therefore observed predominantly temporal restratification.

The two 2020 Seagliders were mounted with unpumped CTDs (conductivity-temperature-depth) provided by Sea-Bird Electronics (CT sail), sampling every 10 s, and Pearldiver was mounted with a Seabird Glider Payload CTD sampling temperature and salinity every 20 s. The Base station from the University of Washington was used to conduct initial processing for sg602 and sg638 (Bennett et al., 2021). In 2022, the two Slocum gliders were mounted with pumped Slocum Glider Payload CTDs with a sampling frequency of 2 s, and their data were processed with PyGlider. Post-processing, sporadic salinity measurement errors were identified within the upper 50–100 m across multiple profiles from all gliders. These spikes can occur from the thermal lag, bubbles in the sensor, biofouling, measurements above the ocean surface, or vehicle stalls, and were manually identified and removed.

Underwater gliders profile the water column in a V-shaped pattern, where the average distance and standard deviation between downward dives for each glider from early winter to restratification were approximately 5 ± 1.3 hr (~4.6 ± 2.5 km). There were a few instances where spacing between glider dives were >8 hr. A total of 10 periods were above this threshold, one of which was during early winter for sg602 and one during convection for Glider 398. Sg638 had the most gaps, with five during early winter and three during convection. These data points were not included in the analysis.

To analyze horizontal and vertical density gradients, glider profiles were linearly interpolated onto a 2-hr horizontal grid and a 5 m vertical grid. The glider distance was interpolated to produce a data set with coordinates in both time and distance, enabling the calculation of lateral gradients. These resolutions were chosen to smooth any noise that may be introduced by instrumentation, while still capturing small-scale features. It is worth noting that gliders can often underestimate lateral gradients due to the limitations of sampling across fronts, as discussed by Thompson et al. (2016). Similarly, the decision to interpolate profiles over time rather than distance may also influence the outputs of buoyancy gradient calculations and equivalent heat flux (Q_{mle}) estimations (Coadou-Chaventon et al., 2024; Swart et al., 2020). Considering this, interpolations over distance were tested and the results across both methods agree. The choice to interpolate over time instead of distance was selected due to the smaller temporal variability across profiles, leading to more consistent interpolation.

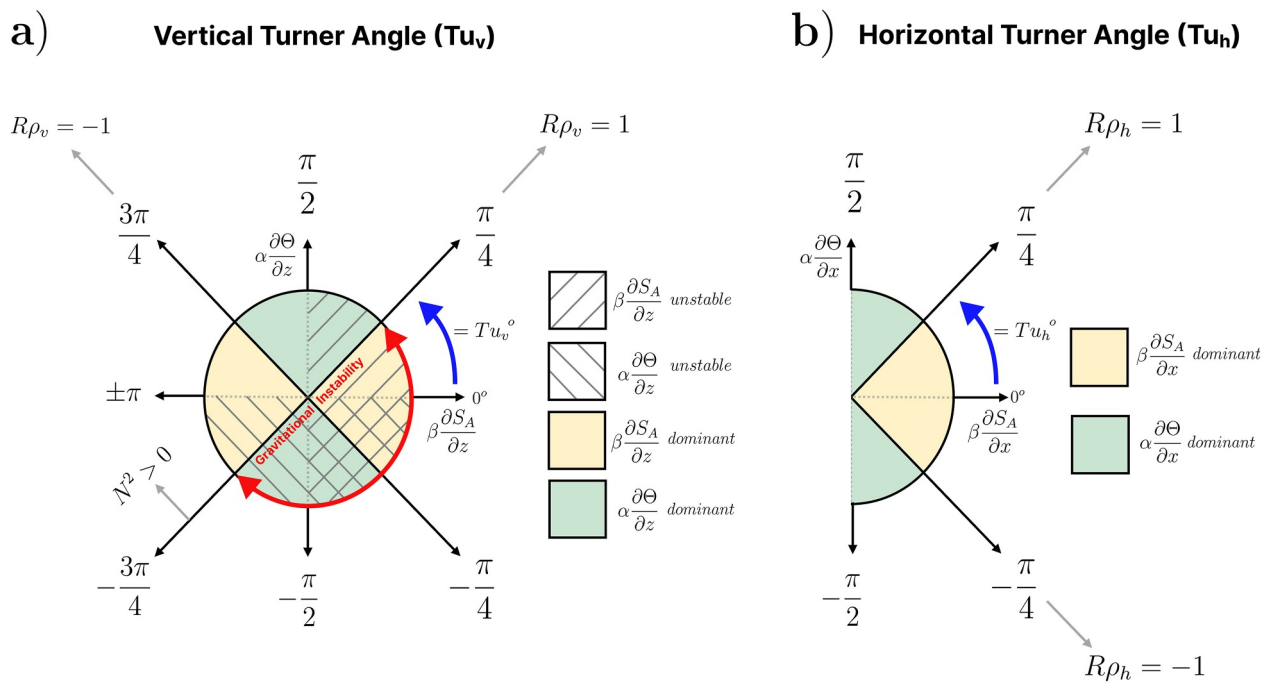

Figure 2. Schematic of the (a) vertical Turner angle, Tu_v, and (b) horizontal Turner angle, Tu_h. Yellow and green sections indicate angles where stratification is primarily influenced by salinity and temperature, respectively. Hatched sections in (a) represent angles where temperature or salinity tend to destabilize the vertical stratification. The small gray arrows indicate whether the effect of temperature and salinity on stratification are fully compensated ($R\rho = 1$) or anti-compensated ($R\rho = -1$).

2.2. Vertical Stratification

By investigating the vertical stratification, we can assess the stability of the water column throughout each winter period by calculating the buoyancy frequency (N^2) using the Gibbs Seawater (GSW) routine (IOC, SCOR, & IAPSO, 2010). The water column is gravitationally unstable for $N^2 < 0$ and stable for $N^2 > 0$ with

$$N^2 = g\left(\beta\frac{\partial S_A}{\partial z} - \alpha\frac{\partial\Theta}{\partial z}\right), \tag{1}$$

where g is the gravitational acceleration, S_A and Θ are the absolute salinity and conservative temperature, α is the thermal expansion coefficient of seawater, and β is the haline contraction coefficient. The relative influence of temperature and salinity on vertical stratification is quantified by the vertical Turner angle (Turner, 1973)

$$Tu_v = \arctan2\left(R\rho_v\right), \tag{2}$$

with $R\rho_v$ the vertical density ratio calculated from

$$R\rho_v = \alpha\frac{\partial\Theta}{\partial z}\left(\beta\frac{\partial S_A}{\partial z}\right)^{-1}. \tag{3}$$

Because of our interest in the dynamics of the MLD and possible entrainment from below, we compare the average conditions within the mixed layer to those 50 m beneath. As such, $\partial\Theta/\partial z$ is defined as the difference in mean conservative temperature within the mixed layer to 50 m beneath the mixed layer, with $\partial z = 50$ m.

The vertical Turner angle covers a range between $-\pi$ and π, which can be separated into a stable or unstable regime (Figure 2a). Stable angles indicate a stably stratified water column under the MLD, and unstable angles suggest the mixed layer is susceptible to further overturning and instability. The angles can be separated into four quadrants that represent whether temperature or salinity has a dominant influence on the vertical density gradient.

2.3. Horizontal Stratification

Analyzing horizontal stratification provides insights into the presence of fronts, which can potentially sustain submesoscale instabilities. By understanding the horizontal structure within the mixed layer, we can establish when and where these fronts exist, if they are driven by temperature or salinity, and whether they link to submesoscale processes that can potentially drive restratification. To identify fronts with the glider data, we first calculate the lateral buoyancy gradient as

$$b_x = g\left(\alpha \frac{\partial \Theta}{\partial x} - \beta \frac{\partial S_A}{\partial x}\right), \tag{4}$$

where ∂x is the distance traveled over each horizontal grid of 2 hr. This calculation of the buoyancy gradient is aligned in the direction of the gliders flight, and therefore will tend to underestimate the real gradient, as discussed in Thompson et al. (2016). Furthermore, density anomalies averaged within the mixed layer are decomposed into temperature and salinity contributions using

$$\rho'_{ml} = \rho_0\left(\beta S_A{}'_{ml} - \alpha \Theta'_{ml}\right), \tag{5}$$

where ρ_0 is a reference density of 1025 kg m^{-3}, and the primes denote the anomaly from a reference temperature of 3.5°C and salinity of 34.85 g kg^{-1} (Clément et al., 2023; Frajka-Williams et al., 2014). This calculation identifies regions where the mixed layer is either warmer or colder, or fresher or saltier than the reference values. To quantify the relationship between temperature and salinity in shaping horizontal fronts, the horizontal Turner angle, Tu_h, is used (Giddy et al., 2021; Spiro Jaeger & Mahadevan, 2018). For Tu_h, the stability criteria applied to Tu_v is not relevant and instead, only the inverse tangent of the horizontal density ratio is required. The horizontal Turner angle is therefore calculated as

$$Tu_h = \arctan\left(R\rho_h\right), \tag{6}$$

where $R\rho_h$ is the horizontal density ratio calculated using

$$R\rho_h = \alpha \frac{\partial \overline{\Theta}}{\partial x}\left(\beta \frac{\partial \overline{S_A}}{\partial x}\right)^{-1}. \tag{7}$$

The overbars represent depth-average values within the mixed layer, and $\frac{\partial \overline{\Theta}}{\partial x}$ represents the horizontal gradient of the depth-averaged conservative temperature in the mixed layer. Angles of Tu_h cover a range between $-\pi/2$ and $\pi/2$. Positive angles capture partially compensated mixed layer density fronts (temperature and salinity are working against each other), whereas negative angles describe anti-compensated fronts (temperature and salinity work together to change density). Consequently, at $\pi/4$ lateral fronts are fully density compensated ($b_x = 0$), and at $-\pi/4$ the fronts are at their strongest. Fronts are mostly driven by salinity if $-\pi/4 < Tu_h < \pi/4$, where angles of 0 represent a front shaped by salinity changes alone. Fronts are temperature-dominated if $|Tu_h| > \pi/4$, and angles of either $-\pi/2$ or $\pi/2$ represent a front driven by a lateral gradient in temperature only (Figure 2b).

2.4. Scales of Variability

To investigate the scales of density variability, the mixed-layer density anomaly (Equation 5) is examined using a wavelet transform based on the Generalized Morse wavelet framework of Lilly and Olhede (2012), characterized by parameters $\gamma = 3$ and $\beta = 2$ (Lilly & Elipot, 2024). This wavelet can represent density variability as a function of both horizontal scale and time. The wavelet analysis can reveal where smaller-scale features are encountered by the gliders and whether they are prominent during restratification. Additionally, wavelet analysis offers a more detailed assessment of the temporal variability of horizontal fronts, revealing how the temperature and salinity contributions to horizontal stratification vary across different periods. Following Coadou-Chaventon et al. (2024), the horizontal density ratio $R\rho_h$ is calculated from wavelet transforms of along track temperature and salinity anomalies. To assess the dominance of either temperature or salinity to fronts over different scales, $|Tu_h|$ is calculated using $|R\rho_h|$ to bound angles between 0 and $\pi/2$. Here, if $0 < |Tu_h| < \pi/4$, horizontal fronts are

dominated by salinity, whereas temperature fronts exist where $\pi/4 < |Tu_h| < \pi/2$. It should be noted that this analysis does not identify whether fronts are compensating or not.

3. Results

3.1. Water Column Structure and Density Anomalies

Glider 398 shows the three winter periods ("early winter," "convection," and "restratification") in the central Labrador Sea (2021–2022, Figure 3). Early winter is characterized by a relatively shallow mixed layer, remaining at approximately 100 m for much of this period. The mixed layer is distinctly warm and fresh (median 3.8°C and 34.8 g kg^{-1}) and has lateral gradients in $|b_x|$ around median 9.5 $\times$ 10^{-9} s^{-2}. Beneath the mixed layer, there is a band of strong vertical stratification (median 1.5 $\times$ 10^{-5} s^{-2}) accompanied by pronounced gradients in $|b_x|$ around median 3.9 $\times$ 10^{-9} s^{-2} (Figures 3e and 3f).

As the winter progresses, the mixed layer deepens, and convection begins. At the onset of this phase in January, Glider 398 observes a large eddy characterized by a strong warm anomaly that extends throughout the measured water column (Figure 3b). Once out of the eddy, the mixed layer becomes progressively cooler, saltier and denser (3.3°C, 34.9 g kg^{-1} and 27.7 kg m^{-3}) and deepens to over 700 m. The lateral buoyancy gradient within the mixed layer weakens relative to early winter, with $|b_x|$ around median 3.3 $\times$ 10^{-9} s^{-2}. Vertical stratification underneath the mixed layer also weakens, indicative of enhanced vertical mixing and entrainment of water from below. During restratification, the MLD is highly variable and stronger $|b_x|$ values re-emerge within the mixed layer (median 4.6 $\times$ 10^{-9} s^{-2}). Mixed layer density reaches its peak during this phase, although the mixed layer is punctuated with regions of lower density that coincide with strong lateral buoyancy gradients and a shoaling MLD.

Above the gliders, the heat flux exhibits a winter cycle (Figure 3a), where the weakest outgoing heat fluxes from the ocean occur during early winter, and the largest during restratification. In early winter for Glider 398, the outgoing heat losses are no stronger than 500 W m^{-2} and the incoming short wave radiation barely reaches 75 W m^{-2}. By the end of the convective period the net outgoing heat losses increase to over 1000 W m^{-2}, driven by an increase in outgoing latent and sensible fluxes. During restratification, the net heat flux becomes more variable, latent and sensible fluxes remain large, and the maximum outgoing net heat loss of 1250 W m^{-2} occurs on 4 March 2022. After this point, less heat is lost from the ocean and the daily short wave radiation cycle becomes prominent after March 13th. For the other gliders (not shown) similar patterns are observed, where early winter heat losses do not exceed around 500 W m^{-2}, except for glider 409 where these almost reach 750 W m^{-2} due to the glider's more northerly position. During convection, the net outgoing heat losses range from 750 W m^{-2} to over 1000 W m^{-2}, with the weakest heat losses around Pearldiver and greatest around glider 409. During restratification the outgoing heat losses remain high, but more variability from the daily short wave radiation is observed due to some of their restratification periods extending into March.

While surface heat fluxes influence water column stability, subsurface processes—such as mixed layer baroclinic instabilities—also contribute to restratification. These submesoscale instabilities can form mixed layer eddies (MLEs) that can restratify the water column through eddy overturning and frontal slumping (Boccaletti et al., 2007; Fox-Kemper et al., 2008). An equivalent heat flux can be calculated to quantify the restratifying capacity using $Q_{mle} = 0.06 b_x^2 H^2 C_p \rho_0 (\alpha g f)^{-1}$, with H the MLD, C_p the heat capacity of seawater and f the Coriolis parameter (Mahadevan et al., 2012). Within the water column, the mixed layer eddy heat flux magnitude increases over the winter period, and is at its largest during restratification with an average magnitude across all gliders of 78 W m^{-2} compared to early winter (33 W m^{-2}) and convection periods (41 W m^{-2}). These heightened values are a result of strengthened lateral buoyancy gradients observed within the mixed layer during the end of winter (Figure 3f), and suggest an enhanced presence of mixed layer instabilities and submesoscale-driven stratification.

To study the density structure, the mixed layer density anomaly is calculated and decomposed into its thermal and haline contributions for each glider (Figure 4). Over winter for all gliders, there is an increase in mixed layer density until the end of the convective period, when this plateaus. This density increase is at times punctuated with short-term variability where the density anomaly (black line) is either more positive (denser) or negative (less dense). During restratification, the density anomaly has pronounced variations toward lighter density caused by warmer and/or fresher conditions within the mixed layer.

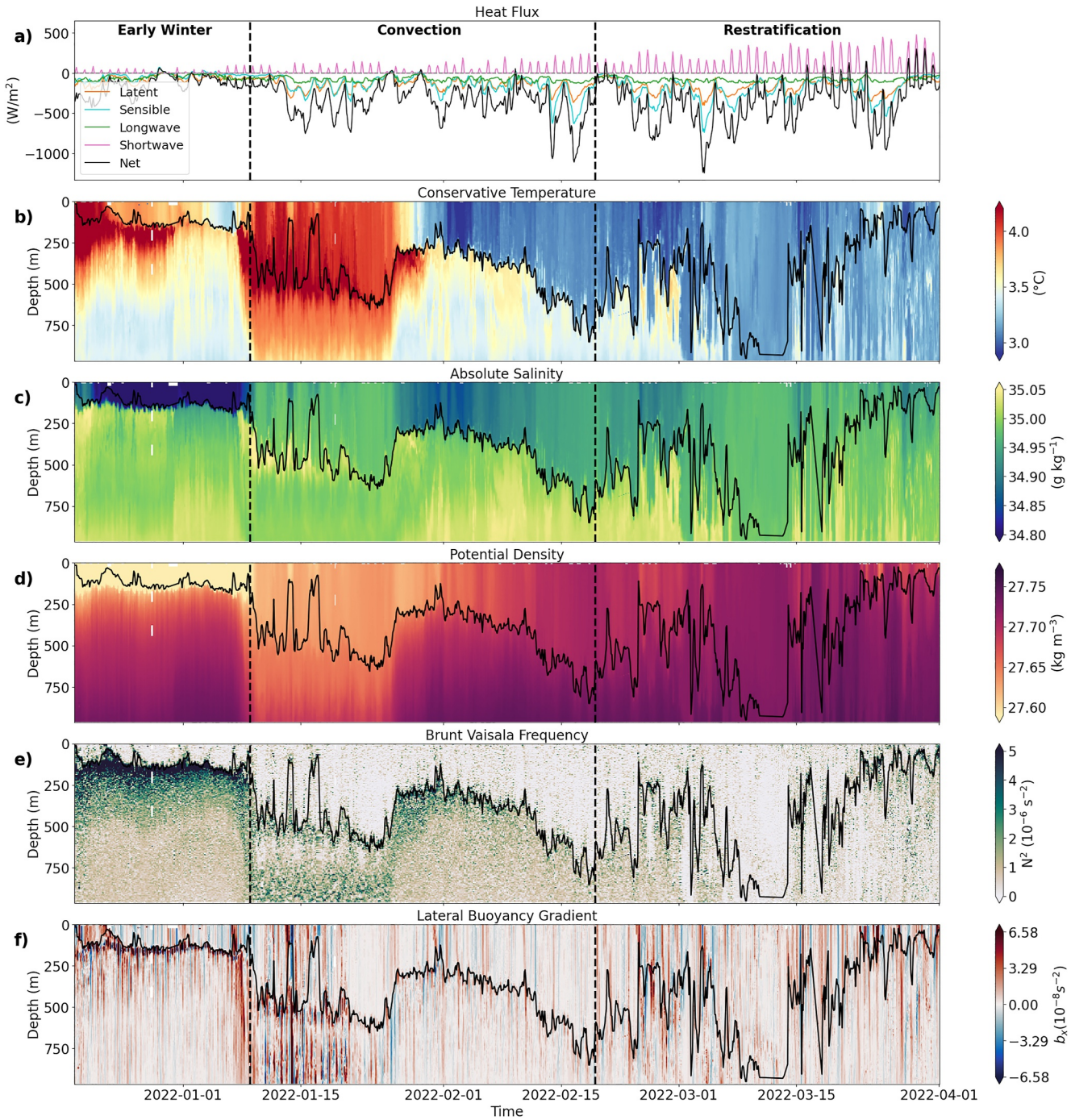

Figure 3. Timeseries of (a) air-sea heat fluxes from ERA5 interpolated to the glider's location. Transects from Glider 398 (winter 2022) of (b) conservative temperature, (c) absolute salinity, (d) potential density (σ_0), (e) buoyancy frequency (N^2) and (f) lateral buoyancy gradient (b_x). Vertical dashed lines separate the transect into "early winter" (left), "convection" (middle), and "restratification" (right), and the mixed layer depth is in black (b–f). Negative heat flux indicates heat loss from the ocean to the atmosphere.

Although anomalies from both fresh and warm conditions persist during restratification, the lateral density structure of the mixed layer is controlled primarily by changes in salinity. Salinity and density anomalies during restratification for glider 398 are strongly correlated ($r = 0.86, p < 0.05$), with slopes between 0.82 and 0.93 for all gliders except sg602 (see Table 1). In comparison, during restratification the temperature anomaly has weaker correlation coefficients within the range of 0.16–0.37, with slopes between 0.07 and 0.18 ($p > 0.05$). Sg602

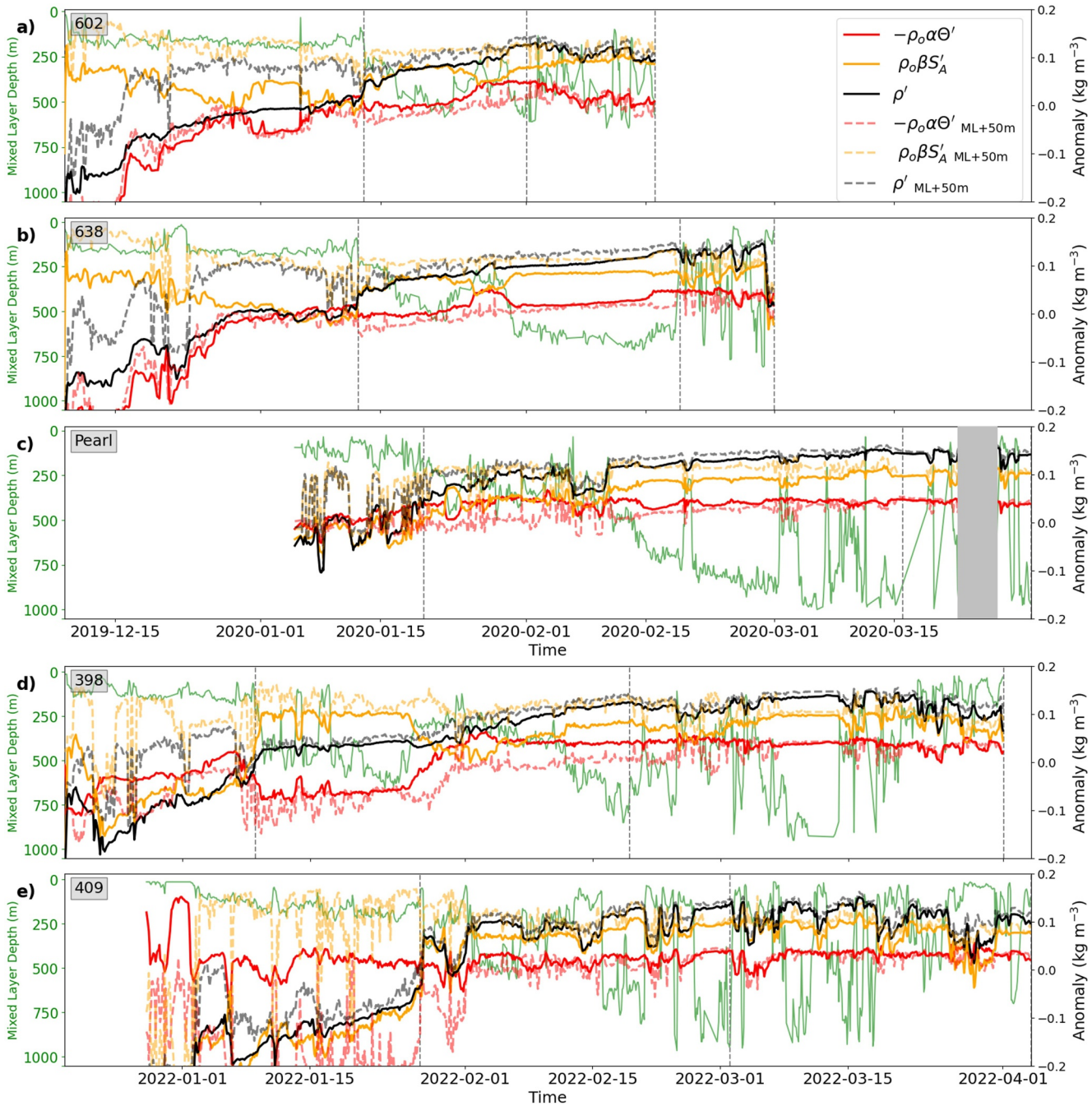

Figure 4. Time series of mixed layer averaged density anomalies (black) and the contributions from temperature (red) and salinity (orange) over the three winter periods separated by the gray vertical dashed lines. Dashed timeseries in each respective color are taken 50 m below the mixed layer depth (MLD). The top three timeseries are from the gliders deployed during winter 2020 (a–c), and the lower two (d, e) from winter 2022. The MLD is displayed in green. Temperature and salinity anomalies are referenced to 3.5 °C and 34.85 g kg^{-1}, respectively. The gray region for Pearldiver represents a gap in the timeseries due to onboard computer issues.

differs in that it crossed waters with a stronger correlation between temperature and density anomalies during restratification ($r = 0.91$, $p < 0.05$, slope = 1.2), and with a weak negative correlation to salinity of −0.36 ($p > 0.05$). This is potentially a consequence of this glider traversing west and measuring restratified waters much earlier than the other gliders, which highlights how thermal and haline relationships may depend on both timing and location in the Labrador Sea. It is worth noting that despite strong correlations for some gliders during

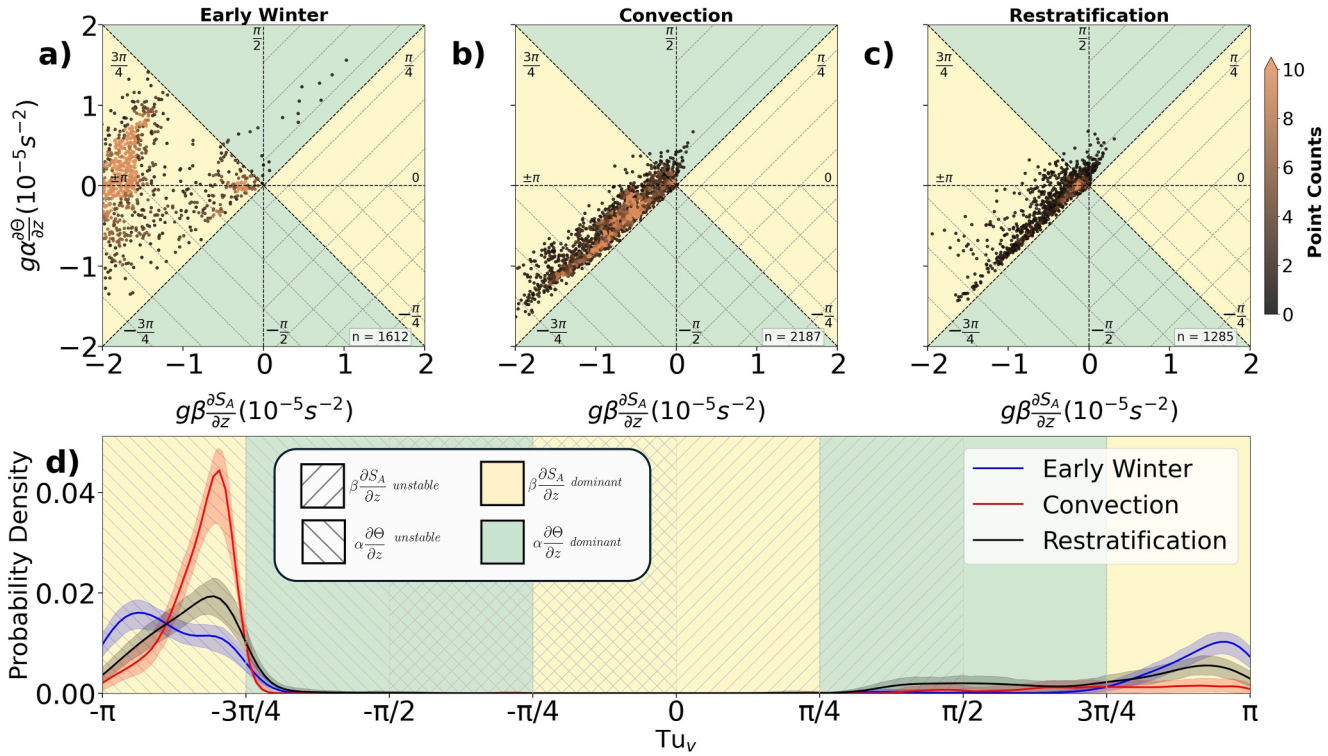

Figure 5. Scatter plots of the vertical gradients of salinity and temperature (times g, β and α, respectively) for all gliders over (a) early winter, (b) convection, and (c) restratification. (d) Distribution of the vertical Turner angle from all gliders in early winter (blue), convection (red), and restratification (black). Temperature or salinity dominates vertical stratification in the green or yellow regions, respectively. The hatched regions demonstrate where salinity or temperature have a destabilizing effect on vertical stratification. The shading around each line in (d) is the 95% confidence interval defined by bootstrapping.

early winter and convection, the result is not significant due to small degrees of freedom, with an average across all gliders and variables of ~6, compared to restratification where more degrees of freedom were sampled (~12).

To characterize vertical stratification, we compare seawater density in the mixed layer to that 50 m below (Figure 4, dashed lines). During early winter, strong vertical density gradients persist between the mixed layer and water below; as winter progresses, the difference between mixed layer density and sub-mixed layer density reduces. These temperature and salinity anomalies are also visible in the section data during the convection period (Figures 3b and 3c), when water 50 m below the mixed layer is warmer and saltier. During restratification, sporadic fresh intrusions coincide with a shoaling MLD. During this time, mixed layer waters are typically colder than below with the exception of for example, glider 398 from 24 March 2022 onwards, as such thermal stratification does not set in until later in the restratification period. This highlights the importance of salinity to density in this region, and how the onset of restratification seems to be initially driven by freshwater intrusions. Later, restratification is maintained by a combination of both warm and fresh mixed layer conditions, when the net heat flux becomes positive.

3.2. Vertical and Lateral Stratification

To quantify the temperature and salinity contributions to stratification at the mixed layer base, we use the vertical Turner angle Tu_v between mixed-layer-averaged properties and properties taken 50 m below the MLD (Figure 5). In early winter, the stratification is stable and salinity dominated, that is, the mixed layer is fresher than below. The large negative values for $g\beta(\partial S_A/\partial z)$ further indicate that stratification is strong. During convection (Figure 5b), enhanced cooling at the ocean surface destabilizes the water column, shown by negative values of $g\alpha(\partial\Theta/\partial z)$. During this time, the density ratio ($R\rho$) is close to 1, and the buoyancy frequency (Figure 3e) reduces meaning vertical stratification at the mixed layer base is weaker and close to instability. During restratification, stratification at the mixed layer base is at its weakest as temperature continues to destabilize, but stratification within the mixed layer increases as a result of salinity (increased N^2), from fresher conditions within the mixed

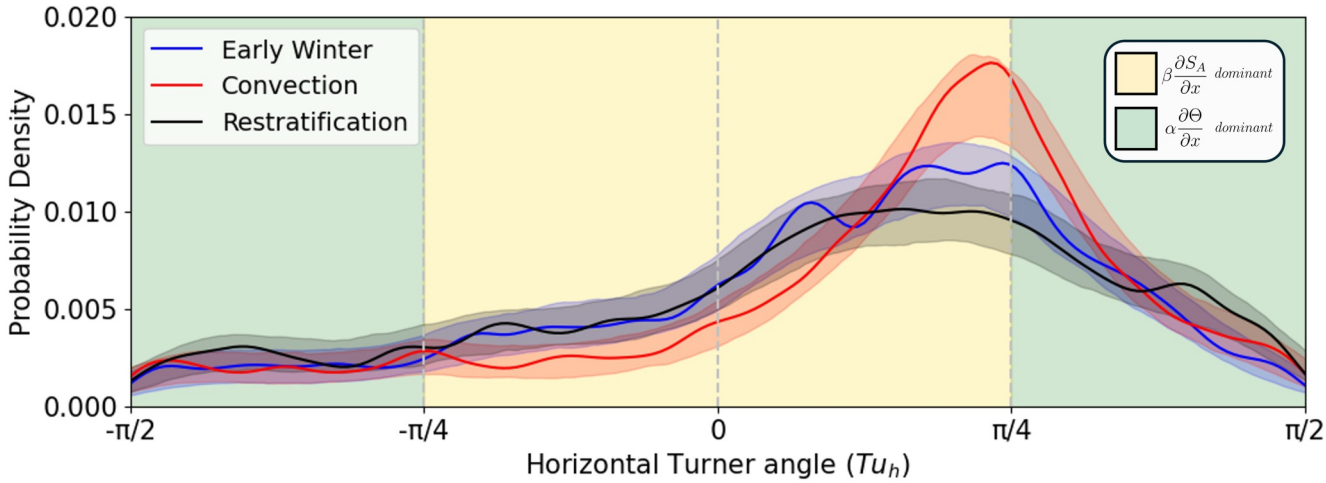

Figure 6. The horizontal Turner angle (Tu_h) distribution within the mixed layer for all gliders for early winter (blue), convection (red), and restratification (black). The shading around each line is the 95% confidence interval defined by bootstrapping. Angles between $-\pi/2$ to 0 represent anti-compensating fronts, and angles between 0 to $\pi/2$ represent compensating fronts.

layer compared to those beneath (Figures 3c and 4). While the increased stratification is predominantly from the haline component, there is an increase in thermal stratification. For Glider 398, these instances are toward the end of winter from 24 March 2022 onwards, aligning with when the ocean begins to gain heat (Figure 3a).

During restratification, the strength of the vertical temperature and salinity gradients is weaker than during convection, as seen by the scatter points moving toward the center of the plot (Figure 5c vs. 5b). This is counter-intuitive to the evidence that more fresh and warm anomalies are within the mixed layer, which would instead suggest stronger gradients in $\beta\frac{\partial S_A}{\partial z}$ or $\alpha\frac{\partial \Theta}{\partial z}$. This is likely a result of enhanced vertical mixing and entrainment during convection, which homogenizes conditions between the mixed layer and water below—therefore reducing vertical gradients for the subsequent period during restratification. This is evident in Figures 3b and 3c, with stronger vertical gradients under the MLD during convection than restratification. Furthermore, this effect is amplified by the shallowing MLD during restratification, as vertical gradients are taken in the remnants of the well mixed convective layer. As a result, the stratification-promoting warm and fresh anomalies present during restratification are sporadic and small in Figure 5c.

To assess the contributions of temperature and salinity to lateral density structure in the mixed layer, we use the horizontal Turner angle Tu_h and compare the three winter periods (Figure 6). As noted previously, values of $Tu_h = \pi/4$ indicate pure compensation (i.e., no lateral density gradients in spite of lateral temperature and salinity gradients), and $Tu_h = -\pi/4$ means temperature and salinity are equally contributing to density gradients. In the Labrador Sea, salinity is the dominant contributor to lateral density gradients during early winter (65% of observations have $-\pi/4 < Tu_h < \pi/4$). During convection, the distribution narrows and the peak shifts toward $Tu_h \approx \pi/4$ indicating weak lateral gradients in density (see also b_x for glider 398 in Figure 3f), where temperature gradients now compensate salinity gradients. During restratification, the conditions closely resemble those of early winter again, where salinity dominates lateral gradients. The intra seasonal patterns of salinity and temperature dominance are consistent with those seen in the vertical (Figure 5d). This highlights a potential connection between horizontal and vertical stratifications, and illustrates how slumping horizontal density fronts can influence the vertical structure of the water column (Boccaletti et al., 2007).

3.3. Scales of Variability

To better understand the drivers of lateral gradients of density in the mixed layer, we determine the scales at which these gradients occur. From this we can assess the dominant scales of fronts potentially acting as a source of restratification, as well as investigate the relative contributions of temperature and salinity at different scales. The separation between submesoscales and mesoscales is not fixed, mesoscales are often defined on the basis of the Rossby radius of deformation (Chelton et al., 1998), which is around 7–8 km within the Labrador Sea (Funk et al., 2009; Gelderloos et al., 2011). This defines horizontal length scales below which local advection is

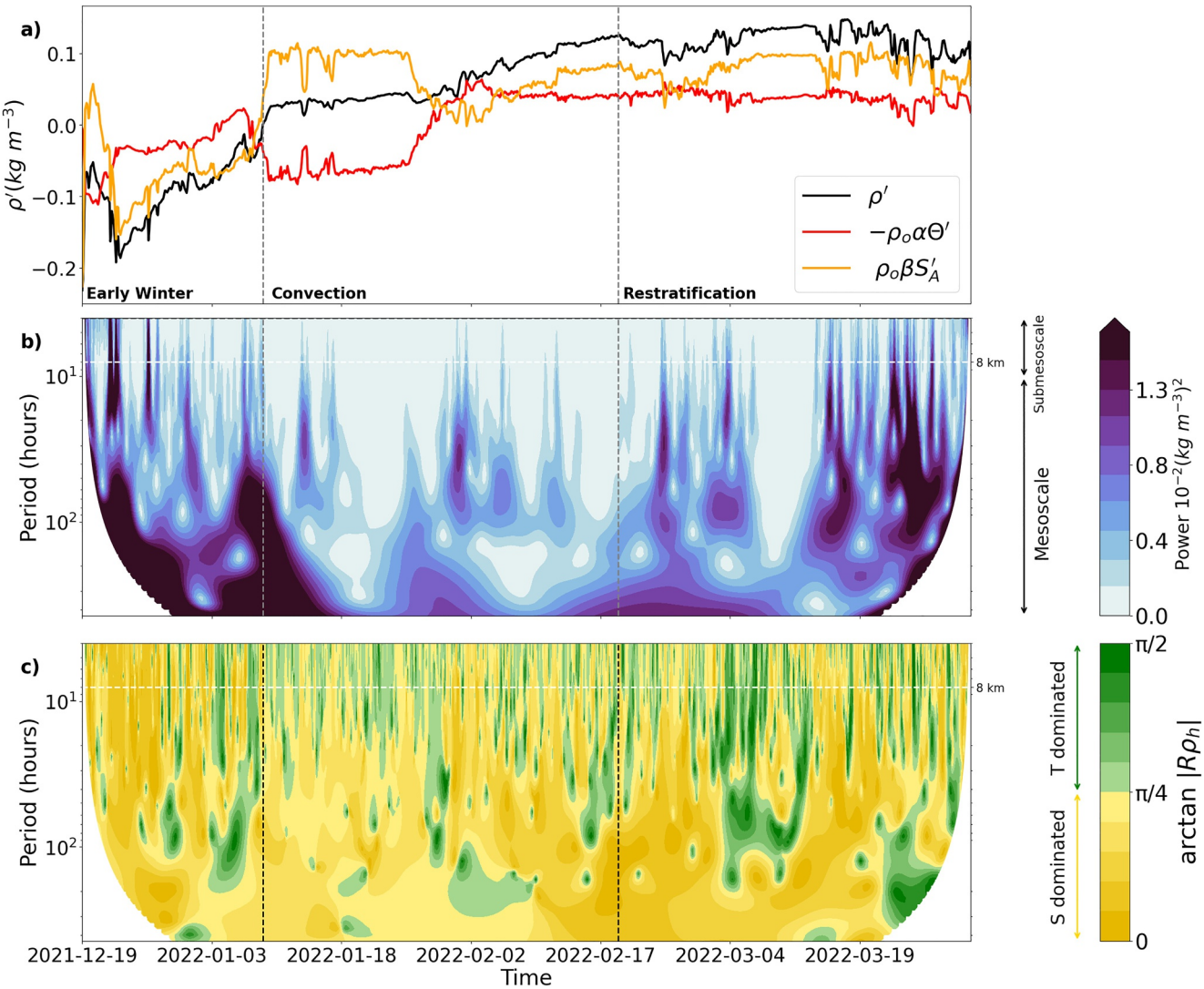

Figure 7. Time series from glider 398 (winter 2022) of (a) mixed layer density, temperature and salinity anomalies, displayed in black, red and orange, respectively (also in Figure 4), (b) wavelet spectra of the density anomaly (black line in a), and (c) the norm of the horizontal density ratio estimated by the wavelet coefficients of the salinity and temperature anomalies. Horizontal density variations are dominated by salinity (yellow, 0 to $\pi/4$) or temperature (green, $\pi/4$ to $\pi/2$). The vertical dashed lines show the separation of the winter periods, and the horizontal dashed white line separates the submesoscale and mesoscale time periods chosen here at ~8 hr (~8 km).

comparably important to planetary rotation, providing a lower bound for the mesoscale range. Comparatively, submesoscale flows are defined as having a horizontal length scale in accordance with the mixed layer Rossby radius of deformation, which is calculated as NH/f with N as the buoyancy frequency within the mixed layer (using $\Delta\rho = 0.01$ kg m^{-3}) (Thomas et al., 2008; Timmermans & Winsor, 2013). The mixed layer Rossby radius calculated from the glider data ranges between 1 and 3 km, which is just below the scope of our spectral analysis. Therefore, this analysis uses the 8 km radius as the approximate separation between submesoscale and mesoscale features. Gliders typically cover 20–25 km per day with 3–4 dive-climb cycles (6–8 profiles). The nominal 8 km separation between submesoscale and mesoscale used here corresponds to a timescale of 8 hr for glider 398 and 409. For Pearldiver, which traveled roughly 20 km per day, 8 km corresponds to 10 hr. The Seagliders sg602 and sg638 traveled more slowly, such that the timescale of separation is 11 hr (sg602) and 12 hr (sg638).

Wavelet analysis enables us to investigate the dominant scales of density variability and how those scales change over time (Figure 7b). For glider 398 and all other gliders (not shown), the greatest density variability occurs during early winter and restratification. During early winter, this variability is associated with increases in mixed layer density (see the power at long periods during early winter, Figure 7b). Density variability is weakest during

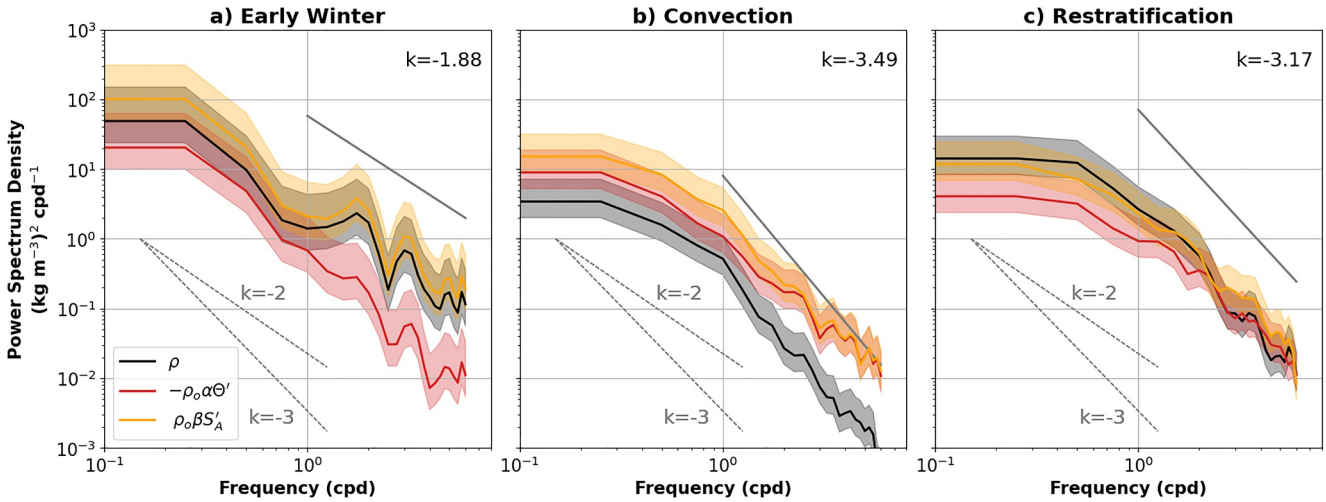

Figure 8. Spectra of glider 398's mixed layer averaged density anomalies (black) and the contributions from salinity (orange) and temperature (red) across (a) early winter, (b) convection and (c) restratification. The 95% confidence interval from each spectra is shaded. Reference slopes of k^{-2} and k^{-3} are shown as gray dotted lines. The slope of the density anomaly is shown as a thick gray line.

convection for all gliders, which is consistent with the temperature-salinity compensation shown by the horizontal Turner angle (Figure 6). To check that the reduced variability during convection is not a consequence of averaging the density anomaly over a larger range of depths (deeper mixed layers during this time), spectra were produced (not shown) using the density anomaly from several depth bins, which all yielded similar results. During restratification, there is a resurgence of energy at both mesoscale and submesoscale periods, and this variability comes from sporadic decreasing ρ' (see the high power at shorter timescales, Figure 7b). This resurgence of energy at both scales could indicate a connection between the mesoscale and submesoscale, where finer scales may be drawing energy from larger scales through stirring (Yu et al., 2024).

To establish the temperature and salinity contributions to lateral density variability, the density ratio $|R\rho_h|$ (Equation 7) is calculated using the wavelet transform of temperature and salinity anomalies depth-averaged in the mixed layer (Figure 7a). This analysis shows the modulus of $R\rho_h$ where lateral density variability is controlled by salinity (yellow) or temperature (green) (Figure 7c), as a function of scale and time. Across all three defined winter periods, salinity is the dominant contributor to lateral density variations at both submesoscale and mesoscale periods. The only exception to this is for sg602 (not shown), where temperature is the dominant control during restratification across both scales. At submesoscales specifically, temperature fronts appear to be more prominent than at the mesoscale; however, salinity remains the dominant contributor within the submesoscale range. For example, at a 7 hr period (<10 km) for glider 398, 66% of fronts over the full winter are salinity-driven, and during restratification these fronts are predominantly fresh (Figure 7a).

The importance of salinity and temperature to density (Figure 4) in the restratification period is depicted by calculating the Welch spectra of the mixed-layer density anomaly (Figure 8). The spectra are computed using consecutive 4 days segments (~80 km), and the slopes over frequencies higher than once per day, to explain energy variance at smaller scales. Across early winter (Figure 8a), the density and salinity slopes are strongly aligned, confirming the salinity dependence of density. During convection, however, both salinity and temperature exhibit greater variance than density, consistent with the stronger density compensation inferred from the horizontal Turner angle during this period (Figure 6). During restratification (Figure 8c), the three slopes are more closely aligned, and this behavior is consistent across all gliders (not shown); however, there is greater power in salinity variance than in temperature, which again demonstrates the preponderance of small-scale, salinity-driven fronts in this region.

The evolution of the spectral slopes over the winter season also informs us about changes in energy transfer as winter progresses. Based on interior quasi geostrophic theory (Charney, 1971) and surface quasi geostrophic theory (Blumen, 1978), steeper slopes $\left(k^{-3}\right)$ infer greater dissipation of energy from larger scales to smaller scales, whereas flatter slopes $\left(k^{-5/3}\right)$ suggest that stirring sharpens fronts (frontogenesis) toward smaller scales.

However, as discussed by Jaeger et al. (2020) observations do not often match this and tend to show slopes more aligned with k^{-2}. The observations from glider 398 (and others, not shown) have slopes on the steeper side tending toward k^{-3}, which based on theory would suggest little energy is maintained at small scales. However, as shown from the wavelet analysis this is not the case, particularly during restratification. While there is a slight flattening of the slope between convection and restratification (Figure 8b vs 8c), the slope remains greater than k^{-3}. Other work, such as that by Timmermans et al. (2012) finds similar steep power spectra when submesoscale processes are actively restratifying the surface mixed layer in the Arctic, and suggests that power laws may differ between high latitude and mid latitude regions. While the spectral slopes here do not match those usually associated with strong frontogenesis, the flattening of the slope between convection and restratification suggests enhanced submesoscale energy which is also shown through the wavelet analysis (Figure 7).

4. Discussion

Hydrographic data from five gliders deployed in the Labrador Sea are used to examine how vertical stratification and horizontal density variability evolve through winter. Observations show that salinity dominates density variability throughout the season, with temperature becoming more influential during convection and at smaller scales. Wavelet analysis indicates elevated submesoscale activity during restratification, with density variability primarily driven by the haline component.

In early winter, the water column is strongly stratified by salinity, shown by a vertical Turner angle distribution dominated by large negative values in $\beta \frac{\partial S_A}{\partial z}$ (Figure 5a). This reflects the Labrador Sea's character as a beta ocean, where cold temperatures reduce the thermal expansion coefficient and amplify the relative importance of salinity to buoyancy (Caneill et al., 2022; Carmack, 2007; Clément et al., 2020; Stewart & Haine, 2016). However, as winter progresses and convection intensifies, surface heat losses (Figure 3) cool and destabilize the upper ocean, deepening the mixed layer and reducing stratification. During this time, temperature partially compensates lateral salinity gradients, creating a more thermally influenced regime with minimal lateral density variability (Figure 6).

During restratification, salinity becomes more influential to mixed layer density. The transition back to haline-driven vertical and horizontal stratification occurs before net surface heat fluxes turn positive (after March 14th, Figure 3a), and while the mixed layer remains colder than underlying waters (Figure 3b). This suggests that restratification precedes atmospheric warming, consistent with previous studies (Mahadevan et al., 2012; du Plessis et al., 2017; Clément et al., 2023, 2024). The stratification is initiated mostly by fresh—but also some warm—water anomalies within the mixed layer. These anomalies are unlikely to come from precipitation or surface heating, considering the limited effect of precipitation (Straneo, 2006) and net negative heat fluxes (Figure 3a), and are therefore more plausibly sourced from lateral transport. Considering glider 398's position toward the western Labrador Sea during restratification, these anomalies likely originate from the relatively fresh Labrador Current. In the future, the Labrador Current is projected to become fresher (Böning et al., 2016), which may strengthen horizontal salinity gradients within the central basin. While further research is needed to determine the precise origin and pathways of these anomalies, future increasing freshwater conditions are likely to weaken deep convection and shorten the convective period.

Spectral analysis shows that fresh and warm anomalies manifest as submesoscale fronts during restratification, as shown by high power at small scales (Figure 7). The prevalence of haline-driven fronts is consistent with results from Drushka et al. (2019), who showed using shipboard thermosalinograph measurements that surface submesoscale fronts in the Labrador Sea are primarily salinity-underpinned. The enhanced presence of these fronts during restratification highlights the potential for submesoscale frontal slumping to occur, which is a known mechanism for rapid restratification (Boccaletti et al., 2007; Clément et al., 2023; Frajka-Williams et al., 2014; Giddy et al., 2021; Gula et al., 2022; Hosegood et al., 2006). The magnitude of the mixed layer eddy heat flux is also the largest during restratification across all gliders, suggestive of enhanced mixed layer eddy activity during this time tending to stratify the water column. While the specific nature of the instabilities cannot be confirmed without further investigation, it is likely that symmetric and mixed layer baroclinic instabilities contribute (Clément et al., 2023). This underscores how small-scale intrusions of mostly fresh, but also warm, waters contribute to the restratification of the Labrador Sea.

A key limitation is that gliders move through both space and time, making it difficult to separate spatial from temporal variability. Glider 398 sampled near the convective edge (Figures 1g and 1h), therefore some variability

may reflect the glider crossing between convective and surrounding waters. However, all gliders observed enhanced small-scale density variability during restratification (Figure 4) without necessarily being at the convective boundary, suggesting this feature is basin-wide. Even if partly spatial, strong horizontal salinity and temperature gradients at the peripheries of the convective patch could themselves trigger instabilities and restratification from the outside in, and future freshening of the boundary regions could enhance boundary-convection gradients and lead to the development of convective eddies along the convective boundary (Clarke & Gascard, 1983; Lilly et al., 2003; Marshall & Schott, 1999).

This study is limited to data from two consecutive winters in close annual succession with deep mixed layers (Yashayaev, 2024); therefore, these results may not represent longer-term conditions. However, as previously noted, Drushka et al. (2019) showed salinity-dominated surface stratification using measurements from 1990 to 2016, suggesting this is a persistent feature of the basin. Considering this, it is worthwhile highlighting that glider sg602 measured a greater dependence of density on temperature during restratification, suggesting that the relative roles of temperature and salinity may vary with timing and location. Depth also affects this relationship (Stewart & Haine, 2016), which highlights the need for more high-resolution sampling across depths and additional winters to capture interannual variability and spatial patterns in stratification.

5. Conclusion

Observations from five gliders in the Labrador Sea across the winters of 2019/20 and 2021/22 demonstrate how salinity is the dominant control on both vertical and horizontal stratifications throughout winter. During early winter, the water column is strongly stratified by salinity. As convection begins, enhanced ocean surface heat losses destabilize stratification and deepen the mixed layer. During this time, temperature becomes more important by having a destabilizing role and offsetting any lateral salinity gradients. During restratification, salinity again becomes more important and has a significant influence on density. This transition back to salinity-driven stratification precedes atmospheric warming and is linked to the presence of fresh intrusions, likely derived from lateral transport. These intrusions appear as submesoscale salinity fronts, which are known to develop instabilities that can rapidly restratify the mixed layer. This highlights the strong salinity dependence of stratification, lateral gradients, and submesoscale dynamics during restratification. Given that future climate projections show increased freshwater inputs from Greenland and the Arctic (Böning et al., 2016; Cosmiso, 2006; Hanna et al., 2008), these findings suggest that freshening rather than warming may have a dominant role triggering restratification in future. Further investigation into the origin and pathways of these freshwater anomalies is essential to understanding their role in submesoscale-mediated restratification and the broader impacts on deep convection.

Conflict of Interest

The authors declare no conflicts of interest relevant to this study.

Availability Statement

The data sets for the sg602 and sg638 TERIFIC gliders are available on SEANOE (https://doi.org/10.17882/82098) (Clément & Frajka-Williams, 2019), and the HOTSeALS (PearlDiver) glider data are available from (https://doi.org/10.17882/79349) (von Oppeln-Bronikowski et al., 2022). The data sets for Gliders 398 and 409 are also available from SEANOE (https://doi.org/10.17882/101369) (Clément & Frajka-Williams, 2021). The PyGlider repository, used to process Gliders 398 and 409 was https://github.com/c-proof/pyglider. The Argo climatology (Roemmich & Gilson, 2009) were collected and made freely available by the International Argo Program and the national programs that contribute to it (http://www.argo.ucsd.edu, http://www.ocean-ops.org). The Argo Program is part of the Global Ocean Observing System. The ERA5 reanalysis can be downloaded from the Copernicus Climate Service (https://cds.climate.copernicus.eu/datasets/reanalysis-era5-single-levels?tab=overview) (Copernicus Climate Change Service & Climate Data Store, 2023). These results contain modified Copernicus Climate Change Service information 2020. Neither the European Commission nor ECMWF is responsible for any use that may be made of the Copernicus information or data it contains.

Acknowledgments
H. Jaques was supported by the Natural Environmental Research Council (NERC) Grant (NE/S007210/1) as part of the INSPIRE Doctoral Training Partnership. M. Oltmanns was supported by the NERC CANARI project (NE/W004984/1) and NERC DIMSUM project (NE/Y005090/1). L. Clément and E. Frajka-Williams were supported by the TERIFIC project that received funding from the European Research Council (ERC) under the European Union's Horizon 2020 research and innovation programme (Grant Agreement 803140). A. Naveira Garabato acknowledges U.K. Research and Innovation guarantee funding for a European Research Council Advanced Grant (EP/X025136/1). The authors also thank two anonymous reviewers for their constructive comments which have helped to greatly improve the manuscript.

References

Argo (2000). Argo float data and metadata from Global Data Assemble Centre (Argo GDAC) [Dataset]. *SEANOE*. https://doi.org/10.17882/42182

Belkin, I. M., Levitus, S., Antonov, J., & Malmberg, S.-A. (1998). "Great Salinity Anomalies" in the North Atlantic. *Progress in Oceanography*, *41*(1), 1–68. https://doi.org/10.1016/S0079-6611(98)00015-9

Bennett, J. S., Stahr, F. R., Eriksen, C. C., Renken, M. C., Snyder, W. E., & Uffelen, L. J. V. (2021). Assessing seaglider model-based position accuracy on an acoustic tracking range. *Journal of Atmospheric and Oceanic Technology*, *38*(6). https://doi.org/10.1175/JTECH-D-20-0091.1

Blumen, W. (1978). Uniform potential vorticity flow: Part I. Theory of wave interactions and two-dimensional turbulence. *Journal of the Atmospheric Sciences*, *35*(5), 774–783. https://doi.org/10.1175/1520-0469(1978)035⟨0774:UPVFPI⟩2.0.CO;2

Boccaletti, G., Ferrari, R., & Fox-Kemper, B. (2007). Mixed layer instabilities and restratification. *Journal of Physical Oceanography*, *37*(9), 2228–2250. https://doi.org/10.1175/JPO3101.1

Böning, C. W., Behrens, E., Biastoch, A., Getzlaff, K., & Bamber, J. L. (2016). Emerging impact of Greenland meltwater on deepwater formation in the North Atlantic Ocean. *Nature Geoscience*, *9*(7), 523–527. https://doi.org/10.1038/ngeo2740

Böning, C. W., Scheinert, M., Dengg, J., Biastoch, A., & Funk, A. (2006). Decadal variability of subpolar gyre transport and its reverberation in the North Atlantic overturning. *Geophysical Research Letters*, *33*(21), 1–5. https://doi.org/10.1029/2006GL026906

Caneill, R., Roquet, F., Madec, G., & Nycander, J. (2022). The polar transition from alpha to beta regions set by a surface buoyancy flux inversion. *Journal of Physical Oceanography*, *52*(8), 1887–1902. https://doi.org/10.1175/JPO-D-21-0295.1

Carmack, E. C. (2007). The alpha/beta ocean distinction: A perspective on freshwater fluxes, convection, nutrients and productivity in high-latitude seas. *Deep-Sea Research Part II*, *54*(23–26), 2578–2598. https://doi.org/10.1016/j.dsr2.2007.08.018

Chanut, J., Barnier, B., Large, G., Debreu, L., Penduff, T., Molines, M., & Mathiot, P. (2008). Mesoscale eddies in the Labrador Sea and their contribution to convection and restratification. *Journal of Physical Oceanography*, *38*(8), 1617–1643. https://doi.org/10.1175/2008JPO3485.1

Charney, J. G. (1971). Geostrophic turbulence. *Journal of the Atmospheric Sciences*, *28*(6), 1087–1095. https://doi.org/10.1175/1520-0469(1971)028⟨1087:GT⟩2.0.CO;2

Chelton, D. B., deSzoeke, R. A., Schlax, M. G., Naggar, K. E., & Siwertz, N. (1998). Geographical variability of the first Baroclinic Rossby radius of deformation. *Journal of Physical Oceanography*, *28*(3), 433–460. https://doi.org/10.1175/1520-0485(1998)028⟨0433:GVOTFB⟩2.0.CO;2

Clarke, R. A., & Gascard, J.-C. (1983). The formation of Labrador Sea water. Part I: Large-scale processes. *Journal of Physical Oceanography*, *13*(10), 1764–1778. https://doi.org/10.1175/1520-0485(1983)013⟨1764:TFOLSW⟩2.0.CO;2

Clément, L., & Frajka-Williams, E. (2019). Terific ocean glider deployments in the labrador sea [Dataset]. *SEANOE*. https://doi.org/10.17882/82098

Clément, L., & Frajka-Williams, E. (2021). Terific 2nd ocean glider deployments in the labrador sea [Dataset]. *SEANOE*. https://doi.org/10.17882/101369

Clément, L., Frajka-Williams, E., Von Oppeln-Bronikowski, N., Goszczko, I., & De Young, B. (2023). Cessation of Labrador Sea convection triggered by distinct fresh and warm (sub)Mesoscale flows. *Journal of Physical Oceanography*, *53*(8), 1959–1977. https://doi.org/10.1175/JPO-D-22-0178.1

Clément, L., McDonagh, E. L., Marzocchi, A., & Nurser, A. J. G. (2020). Signature of ocean warming at the mixed layer base. *Geophysical Research Letters*, *47*(1), 1–10. https://doi.org/10.1029/2019GL086269

Clément, L., Merckelbach, L., & Frajka-Williams, E. (2024). Turbulent vertical velocities in labrador sea convection. *Geophysical Research Letters*, *51*(21), 1–11. https://doi.org/10.1029/2024GL110318

Coadou-Chaventon, S., Speich, S., Zhang, D., Rocha, C. B., & Swart, S. (2024). Oceanic fronts driven by the amazon freshwater plume and their thermohaline compensation at the submesoscale. *Journal of Geophysical Research: Oceans*, *129*(7), 1–23. https://doi.org/10.1029/2024JC021326

Copernicus Climate Change Service, & Climate Data Store. (2023). ERA5 hourly data on single levels from 1940 to present [Dataset]. https://doi.org/10.24381/cds.adbb2d47

Cosmiso, J. (2006). Arctic warming signals from satellite observations. *Weather*, *61*(3), 62–92. https://doi.org/10.1256/wea.222.05

Curry, R. G., McCartney, M. S., & Joyce, T. M. (1998). Oceanic transport of subpolar climate signals to mid-depth subtropical waters. *Nature*, *391*(6667), 575–577. https://doi.org/10.1038/35356

Drushka, K., Asher, W. E., Sprintall, J., Gille, S. T., & Hoang, C. (2019). Global patterns of submesoscale surface salinity variability. *Journal of Physical Oceanography*, *49*(7), 1669–1685. https://doi.org/10.1175/JPO-D-19-0018.1

du Plessis, M., Swart, S., Ansorge, I. J., & Mahadevan, A. (2017). Submesoscale processes promote seasonal restratification in the Subantarctic Ocean. *Journal of Geophysical Research: Oceans*, *122*(4), 2960–2975. https://doi.org/10.1002/2016JC012494

du Plessis, M., Swart, S., Ansorge, I. J., Mahadevan, A., & Thompson, A. F. (2019). Southern Ocean seasonal restratification delayed by submesoscale wind–front interactions. *Journal of Physical Oceanography*, *49*(4), 1035–1053. https://doi.org/10.1175/JPO-D-18-0136.1

Eden, C., & Böning, C. (2002). Sources of Eddy kinetic energy in the Labrador Sea. *Journal of Physical Oceanography*, *32*(12), 3346–3363. https://doi.org/10.1175/1520-0485(2002)032⟨3346:SOEKEI⟩2.0.CO;2

Fox-Kemper, B., Ferrari, R., & Hallberg, R. (2008). Parameterization of mixed layer eddies. Part I: Theory and diagnosis. *Journal of Physical Oceanography*, *38*(6), 1145–1165. https://doi.org/10.1175/2007JPO3792.1

Frajka-Williams, E., Rhines, P. B., & Eriksen, C. C. (2014). Horizontal stratification during deep convection in the Labrador Sea. *Journal of Physical Oceanography*, *44*(1), 220–228. https://doi.org/10.1175/JPO-D-13-069.1

Funk, A., Brandt, P., & Fischer, T. (2009). Eddy diffusivities estimated from observations in the Labrador Sea. *Journal of Geophysical Research*, *114*(C4). https://doi.org/10.1029/2008JC005098

Gelderloos, R., Katsman, C. A., & Drijfhout, S. S. (2011). Assessing the roles of three eddy types in restratifying the labrador Sea after deep convection. *Journal of Physical Oceanography*, *41*(11), 2102–2119. https://doi.org/10.1175/JPO-D-11-054.1

Gelderloos, R., Straneo, F., & Katsman, C. A. (2012). Mechanisms behind the temporary shutdown of deep convection in the Labrador Sea: Lessons from the great salinity Anomaly years 1968-71. *Journal of Climate*, *25*(19), 6743–6755. https://doi.org/10.1175/JCLI-D-11-00549.1

Giddy, I., Swart, S., du Plessis, M., Thompson, A. F., & Nicholson, S.-A. (2021). Stirring of sea-ice meltwater enhances submesoscale fronts in the Southern Ocean. *Journal of Geophysical Research: Oceans*, *126*(4), 1–24. https://doi.org/10.1029/2020JC016814

Gula, J., Taylor, J., Shcherbina, A., & Mahadevan, A. (2022). Submesoscale processes and mixing. In *Ocean mixing* (pp. 181–214). Elsevier. https://doi.org/10.1016/B978-0-12-821512-8.00015-3

Hanna, E., Huybrechts, P., Steffen, K., Cappelen, J., Huff, R., Shuman, C., et al. (2008). Increased runoff from melt from the Greenland ice sheet: A response to global warming. *Journal of Climate*, *21*(2), 331–341. https://doi.org/10.1175/2007JCLI1964.1

Hátún, H., Eriksen, C. C., & Rhines, P. B. (2007). Buoyant eddies entering the Labrador Sea observed with gliders and altimetry. *Journal of Physical Oceanography*, *37*(12), 2838–2854. https://doi.org/10.1175/2007JPO3567.1

Hosegood, P., Gregg, M. C., & Alford, M. H. (2006). Sub-mesoscale lateral density structure in the oceanic surface mixed layer. *Geophysical Research Letters*, *33*(22), 1–6. https://doi.org/10.1029/2006GL026797

IOC, SCOR, & IAPSO. (2010). The international thermodynamic equation of seawater - 2010: Calculation and use of thermodynamic properties. *UNESCO*, *56*(148), 1–207.

Jaeger, G. S., MacKinnon, J. A., Lucas, A. J., Shroyer, E., Nash, J., Tandon, A., et al. (2020). How spice is stirred in the Bay of Bengal. *Journal of Physical Oceanography*, *50*(9), 2669–2688. https://doi.org/10.1175/JPO-D-19-0077.1

Jones, H., & Marshall, J. (1997). Restratification after deep convection. *Journal of Physical Oceanography*, *27*(10), 2276–2287. https://doi.org/10.1175/1520-0485(1997)027<2276:radc>2.0.co;2

Katsman, C. A., Spall, M. A., & Pickart, R. S. (2004). Boundary current eddies and their role in the restratification of the Labrador Sea. *Journal of Physical Oceanography*, *34*(9), 1967–1983. https://doi.org/10.1175/1520-0485(2004)034<1967:bceatr>2.0.co;2

Lavender, K. L., Davis, R. E., & Owens, W. B. (2000). Mid-depth recirculation observed in the interior Labrador and Irminger seas by direct velocity measurements. *Nature*, *407*(6800), 66–69. https://doi.org/10.1038/35024048

Lazier, J. (1980). Oceanographic conditions at ocean weather Ship Bravo, 1964–1974. *Atmosphere-Ocean*, *18*(3), 227–238. https://doi.org/10.1080/07055900.1980.9649089

Lazier, J., Hendry, R., Clarke, A., Yashayaev, I., & Rhines, P. (2002). Convection and restratification in the Labrador Sea, 1990–2000. *Deep Sea Research Part I: Oceanographic Research Papers*, *49*(10), 1819–1835. https://doi.org/10.1016/S0967-0637(02)00064-X

Lilly, J., & Elipot, S. (2024). jonathanlilly/jLab: jLab v1.7.3 (Version v1.7.3) [Computer software]. *Zenodo*. https://doi.org/10.5281/ZENODO.4547006

Lilly, J. M., & Olhede, S. C. (2012). Generalized morse wavelets as a superfamily of analytic wavelets. *IEEE Transactions on Signal Processing*, *60*(11), 6036–6041. https://doi.org/10.1109/TSP.2012.2210890

Lilly, J. M., Rhines, P. B., Schott, F., Lavender, K., Lazier, J., Send, U., & D'Asaro, E. (2003). Observations of the Labrador Sea eddy field. *Progress in Oceanography*, *59*(1), 75–176. https://doi.org/10.1016/j.pocean.2003.08.013

Mahadevan, A., D'Asaro, E., Lee, C., & Perry, M. J. (2012). Eddy-driven stratification initiates north Atlantic spring phytoplankton blooms. *Science*, *337*(6090), 54–58. https://doi.org/10.1126/science.1218740

Marshall, J., Dobson, F., Moore, K., Rhines, P., Visbeck, M., D'Asaro, E., & Smethie, W. (1998). The labrador sea deep convection experiment. *Bulletin of the American Meteorological Society*, *79*(10), 2033–2058. https://doi.org/10.1175/1520-0477(1998)079%3C2033:TLSDCE%3E2.0.CO;2

Marshall, J., & Schott, F. (1999). Open-ocean convection: Observations, theory, and models. *Reviews of Geophysics*, *37*(1), 1–64. https://doi.org/10.1029/98RG02739

NOAA National Geophysical Data Center. (2009). Etopo1 arc-minute global relief model [Dataset]. *NOAA National Centers for Enviromental Information*. https://www.ngdc.noaa.gov/mgg/global/relief/ETOPO1/tiled/

Pickart, R. S., Torres, D. J., & Clarke, R. A. (2002). Hydrography of the Labrador Sea during active convection. *Journal of Physical Oceanography*, *32*(2), 428–457. https://doi.org/10.1175/1520-0485(2002)032<0428:hotlsd>2.0.co;2

Piron, A., Thierry, V., Mercier, H., & Caniaux, G. (2016). Argo float observations of basin-scale deep convection in the Irminger sea during winter 2011–2012. *Deep Sea Research Part I: Oceanographic Research Papers*, *109*, 76–90. https://doi.org/10.1016/j.dsr.2015.12.012

Prater, M. D. (2002). Eddies in the labrador Sea as observed by profiling RAFOS floats and remote sensing. *Journal of Physical Oceanography*, *32*(2), 411–427. https://doi.org/10.1175/1520-0485(2002)032<0411:eitlsa>2.0.co;2

Rhein, M., Steinfeldt, R., Kieke, D., Stendardo, I., & Yashayaev, I. (2017). Ventilation variability of Labrador Sea Water and its impact on oxygen and anthropogenic carbon: A review. *Philosophical Transactions of the Royal Society A: Mathematical, Physical and Engineering Sciences*, *375*(2102), 1–17. https://doi.org/10.1098/rsta.2016.0321

Rieck, J. K., Böning, C. W., & Getzlaff, K. (2019). The nature of Eddy kinetic energy in the Labrador Sea: Different types of mesoscale eddies, their temporal variability, and impact on deep convection. *Journal of Physical Oceanography*, *49*(8), 2075–2094. https://doi.org/10.1175/JPO-D-18-0243.1

Roemmich, D., & Gilson, J. (2009). The 2004–2008 mean and annual cycle of temperature, salinity, and steric height in the global ocean from the argo program. *Progress in Oceanography*, *82*(2), 81–100. https://doi.org/10.1016/j.pocean.2009.03.004

Sabine, C., Feely, R., Gruber, N., Key, R., Lee, K., Bullister, J., et al. (2004). The oceanic sink for anthropogenic CO2. *Science*, *305*(5682), 367–371. https://doi.org/10.1126/science.1097403

Schulze, L. M., Pickart, R. S., & Moore, G. W. K. (2016). Atmospheric forcing during active convection in the Labrador Sea and its impact on mixed-layer depth. *Journal of Geophysical Research: Oceans*, *121*(9), 6978–6992. https://doi.org/10.1002/2015JC011607

Spall, M. A. (2004). Boundary currents and watermass transformation in marginal seas. *Journal of Physical Oceanography*, *34*(5), 1197–1213. https://doi.org/10.1175/1520-0485(2004)034<1197:bcawti>2.0.co;2

Spiro Jaeger, G., & Mahadevan, A. (2018). Submesoscale-selective compensation of fronts in a salinity-stratified ocean. *Science Advances*, *4*(2), 1–9. https://doi.org/10.1126/sciadv.1701504

Stewart, K. D., & Haine, T. W. N. (2016). Thermobaricity in the transition zones between alpha and beta oceans. *Journal of Physical Oceanography*, *46*(6), 1805–1821. https://doi.org/10.1175/JPO-D-16-0017.1

Straneo, F. (2006). Heat and freshwater transport through the central Labrador Sea. *Journal of Physical Oceanography*, *36*(4), 606–628. https://doi.org/10.1175/JPO2875.1

Swart, S., du Plessis, M. D., Thompson, A. F., Biddle, L. C., Giddy, I., Linders, T., et al. (2020). Submesoscale fronts in the antarctic marginal ice zone and their response to wind forcing. *Geophysical Research Letters*, *47*(6), 1–10. https://doi.org/10.1029/2019GL086649

Talley, L. D. (2003). Shallow, intermediate, and deep overturning components of the global heat budget. *Journal of Physical Oceanography*, *33*(3), 530–560. https://doi.org/10.1175/1520-0485(2003)033<0530:siadoc>2.0.co;2

Thomas, L. N., Tandon, A., & Mahadevan, A. (2008). Submesoscale processes and dynamics. In *Ocean modeling in an eddying regime* (pp. 17–38). American Geophysical Union (AGU). https://doi.org/10.1029/177GM04

Thompson, A. F., Lazar, A., Buckingham, C., Garabato, A. C. N., Damerell, G. M., & Heywood, K. J. (2016). Open-ocean submesoscale motions: A full seasonal cycle of mixed layer instabilities from gliders. *Journal of Physical Oceanography*, *46*(4), 1285–1307. https://doi.org/10.1175/JPO-D-15-0170.1

Timmermans, M.-L., Cole, S., & Toole, J. (2012). Horizontal density structure and restratification of the Arctic Ocean surface layer. *Journal of Physical Oceanography*, *42*(4), 659–668. https://doi.org/10.1175/JPO-D-11-0125.1

Timmermans, M.-L., & Winsor, P. (2013). Scales of horizontal density structure in the Chukchi Sea surface layer. *Continental Shelf Research*, *52*, 39–45. https://doi.org/10.1016/j.csr.2012.10.015

Turner, J. (1973). *Buoyancy effects in fluids*. Cambridge University press. https://doi.org/10.1017/CBO9780511608827

Uppala, S. M., Kållberg, P. W., Simmons, A. J., Andrae, U., Bechtold, V. D. C., Fiorino, M., et al. (2005). The ERA-40 re-analysis. *Quarterly Journal of the Royal Meteorological Society*, *131*(612), 2961–3012. https://doi.org/10.1256/qj.04.176

Våge, K., Pickart, R. S., Thierry, V., Reverdin, G., Lee, C. M., Petrie, B., et al. (2009). Surprising return of deep convection to the subpolar North Atlantic Ocean in winter 2007–2008. *Nature Geoscience*, *2*(1), 67–72. https://doi.org/10.1038/ngeo382

von Oppeln-Bronikowski, N., de Young, B., Bachmayer, R., Palter, J., Claus, B., Zhou, M., et al. (2022). Memorial university ocean glider deployments: 2005 – present [Dataset]. *SEANOE*. https://doi.org/10.17882/79349

Yashayaev, I. (2024). Intensification and shutdown of deep convection in the Labrador Sea were caused by changes in atmospheric and freshwater dynamics. *Communications Earth & Environment*, *5*(1), 1–23. https://doi.org/10.1038/s43247-024-01296-9

Yashayaev, I., & Loder, J. W. (2016). Recurrent replenishment of Labrador Sea water and associated decadal-scale variability. *Journal of Geophysical Research: Oceans*, *121*(11), 8095–8114. https://doi.org/10.1002/2016JC012046

Yashayaev, I., van Aken, H., Holliday, P., & Bersch, M. (2007). Transformation of the Labrador Sea water in the subpolar North Atlantic. *Geophysical Research Letters*, *34*(22), 1–8. https://doi.org/10.1029/2007GL031812

Yeager, S., Castruccio, F., Chang, P., Danabasoglu, G., Maroon, E., Small, J., et al. (2021). An outsized role for the Labrador Sea in the multidecadal variability of the Atlantic overturning circulation. *Science Advances*, *7*(41), 1–14. https://doi.org/10.1126/sciadv.abh3592

Yu, X., Barkan, R., & Naveira Garabato, A. C. (2024). Intensification of submesoscale frontogenesis and forward energy cascade driven by upper-ocean convergent flows. *Nature Communications*, *15*(1), 9214. https://doi.org/10.1038/s41467-024-53551-4